Energy Conversion and Management 136 (2017) 307–317

Contents lists available at ScienceDirect

Energy Conversion and Management

journal homepage: www.elsevier.com/locate/enconman

Investigation of the performance improvement in decreasing aspect ratio interdigitated flow field PEMFCs

Nathanial J. Cooper [a], Anthony D. Santamaria [b], Maxwell K. Becton [a], Jae Wan Park [a,*]

[a] Department of Mechanical and Aerospace Engineering, University of California, One Shields Ave., Davis, CA 95616-5294, United States
[b] Mechanical Engineering, Western New England University, 1215 Wilbraham Road, Springfield, MA 01119, United States

ARTICLE INFO

Article history:
Received 12 October 2016
Received in revised form 27 December 2016
Accepted 3 January 2017
Available online 18 January 2017

Keywords:
Interdigitated
Aspect ratio
PEM fuel cells
Water
Cross flow
Neutron radiography

ABSTRACT

The goal of this study was to determine the main cause of performance improvement in decreasing aspect ratio interdigitated flow fields, where aspect ratio is the channel length to width ratio. An experimental test cell with an interdigitated flow field operated under various aspect ratios found increasing net power densities with decreasing aspect ratio, after accounting for parasitic pump losses. In-situ neutron radiography found there was more water present in high aspect ratio flow field designs than in low aspect ratio designs. It also found more water in the 1.5/2 stoichiometry conditions than in the 2/4 stoichiometry conditions further indicating liquid water is a probable cause of performance changes. A single phase model used to determine the difference in power from the changing distribution of cross flow found decreasing aspect ratio resulted in higher overall performance. The experiment had significantly greater losses in power density with increasing aspect ratio, indicating liquid water removal was the major contributor to the improvement in net power density rather than the distribution of cross flow. Designers of PEMFCs should use a low aspect ratio design for interdigitated flow fields, or include a water removal mechanism for situations where high aspect ratio is required.

1. Introduction

Proton exchange membrane fuel cells (PEMFCs) have great potential as a future power system in both stationary and transportation applications. The area of flow field design still needs to be more fully explored to improve the power density and understand the effect on fuel cell performance. Interdigitated flow fields force convective transport between channels, through the gas diffusion layer (GDL) and catalyst layer (CL), also known as cross flow. This convective transport between channels reduces the concentration overpotential [1]. Cross flow in interdigitated flow fields carries fresh reactants closer to the catalyst layer, reducing the required diffusion length, allowing for faster transport of fresh reactant. This reduction in concentration losses allows interdigitated designs to reach higher limiting current densities than equivalent parallel designs [2]. While there is an increase in pumping pressure required to drive the reactants, interdigitated designs tend to have a higher net power, after subtracting pumping losses, than equivalent parallel flow designs [2,3]. There has been limited experimental work on cross flow distribution effects in interdigitated flow fields, however.

There has been work of interest regarding cross flow on the performance effect of induced cross flow in parallel flow fields. Bachman et al. [4] designed a parallel flow field where the outlet of one set of channels could be regulated, inducing cross flow. They found that at performance improved in the partially blocked cases, particularly at elevated stoichiometry. Tong et al. [5] extended this work, designing a hybrid parallel/interdigitated flow field, with regulators at the inlet of one subset of channels and at the outlet of other subset of channels. The hybrid flow field achieved elevated performance compared to both parallel and interdigitated flow fields. Alternative flow fields and operational styles which make use of cross flow have been examined as well [6,7]. Taira and Liu [8] examined the effect of humidity on the cross flow induced pressure drop across a gas diffusion layer. Santamaria et al. [9] examined the effect of cross flow velocity on water distribution and accumulation in interdigitated flow field fuel cells.

Modeling of PEMFCs has become more commonplace and useful as computing power becomes more accessible [10–12]. Kanezaki et al. [13] found that cross flow rate is strongly related to the catalyst layer reactant concentration and further that increased water removal rates and lower concentration overpotentials are due to increased cross flow of interdigitated flow fields. Arato et al. [14]

* Corresponding author.
E-mail addresses: natcooper@ucdavis.edu (N.J. Cooper), mkbecton@ucdavis.edu (M.K. Becton), jwpark@ucdavis.edu (J.W. Park).

http://dx.doi.org/10.1016/j.enconman.2017.01.005
0196-8904/

Nomenclature

A_c	cathodic Tafel slope, mV
A_s	active specific surface area, m^{-1}
C_p	specific heat of air, J/kg K
d	depth, mm
$\dot{E}$	power, mW
I	neutron flux
k	specific heat ratio
L/D ratio	length over diameter ratio
L	length, cm
p	pressure, Pa
T	temperature, K
U	air velocity, cm/s
V	voltage, V
v	volume fraction of electrolyte
w	width, mm
x	material thickness, mm

Greek letters

Σ_i	macroscopic cross section (neutron attenuation coefficient), m^{-1}
α	transfer coefficient
ε	porosity
η	pump efficiency
κ	permeability, m^2
σ	conductivity, S/m

Subscripts/superscripts

0	initial
anode	anode
atm	atmospheric
cathode	cathode
cell	cell
ch	channel
comp	compressed GDL
D	dry
dew	dew point
exit	exit
inlet	inlet
land	land
mem	membrane
pump	pump
sys	system
W	wet

Abbreviations used in text

AR	Aspect Ratio
ANOVA	Analysis of Variance
CL	Catalyst Layer
GDL	Gas Diffusion Layer
MEA	Membrane Electrode Assembly
MPL	Microporous Layer
PEMFC	Polymer Electrolyte Membrane Fuel Cell

performed simulations on interdigitated and partially interdigitated PEMFCs with varying dimensionless permeability conditions. Extensive optimization simulations by Grujicic et al. [15] found reduced channel length and width result in increased performance, all else being equal. This analysis helped to further confirm the relationship between reactant concentration in the catalyst layer and overall performance. Khazaee and Sabadbafan [16] developed a simulation which examines the effect of cross flow in serpentine flow field fuel cells, finding the 4-channel serpentine flow field outperformed a 1-channel flow field. Mahmoudi et al. [17] developed a model to examine the effect of the compression under lands in interdigitated flow fields. Given the relative dearth of experimental work, these simulations remain instructive, but not the final word on the topic.

Neutron radiography is a non-invasive method of examining internal features using thermal neutrons. In particular, neutron radiography can be used to examine the in-situ water distribution within a PEMFC [18–20]. This information is useful for designers, as previous studies have shown that the presence of liquid water within a fuel cell degrades performance [21,22]. For example, Spernjak et al. used neutron imaging to compare the water content within parallel, single serpentine and interdigitated flow fields [23], while Owejan et al. examined the level of saturation within channels of an interdigitated fuel cell [24]. Hickner et al. examined the water content distribution of a PEMFC under a range of humidity values and local temperatures [25].

Investigations into the relationship between aspect ratio and net power density for parallel flow fields have been performed both computationally and experimentally [26,27]. The relationship between aspect ratio (AR), cross flow distribution and net power density in interdigitated flow fields is less completely understood, and less fully explored. Given previous work on cross flow and internal cell pressure of interdigitated flow fields [28], it is of interest to examine the effect of varying aspect ratio on cross flow in interdigitated cells. Previous work has found that decreasing the length of channels in an interdigitated fuel cell, thus decreasing the aspect ratio, causes an increase in the net power density of the fuel cell [29]. It also found that increasing the aspect ratio led to an uneven distribution of cross flow down the length of the fuel cell. The effect of aspect ratio on cell performance is examined thoroughly by the previous work, but the cause of this effect has not been fully examined.

The current work seeks to build on this previous work to understand the cause of the increase in net power density as aspect ratio decreases. The goal of this study is to examine the potential causes of this change in net power density, including in-situ water distribution and the uneven distribution of cross flow as aspect ratio changes. Since the previous work uses stoichiometry as an examined variable, stoichiometry will be examined as well. Fuel cell stack designers will inevitably be faced with limitations on size and shape in the design of the units they create. These limitations hold the potential to limit the power produced by a stack. Understanding the cause of power density changes in light of changes in aspect ratio allows for the mitigation of these issues and provides the potential for high power densities regardless of shape constraints.

In this study, an interdigitated flow field PEMFC which could switch between 5 cm, 15 cm and 25 cm in length (with fixed channel widths, channel depths and land widths of 1 mm) was designed and tested to determine the improvement in power density that comes with decreasing length. A statistical analysis of aspect ratio and stoichiometry, based on the experimental results, helped to clarify the effect of these factors on performance. Neutron radiography was performed on the high and low aspect ratio flow fields to determine whether a difference in water buildup played a role major in performance improvement. Measuring the extent of water buildup does not, however, provide an exact measure of the corresponding decrease in power density due strictly to water

buildup. There may be other causes of changing power density in the cell, including the uneven distribution of cross flow, as noted in [29]. To determine the extent of performance change due strictly to uneven cross flow distribution, a single phase computational study was performed which examined the power generated for the interdigitated cell at each aspect ratio that was examined experimentally. The associated decrease in power density for increasing aspect ratio designs which is not attributed to the uneven cross flow could then be attributed to the presence of liquid water, as observed in the neutron imaging.

2. Experimental setup

2.1. Test cell construction

A previous study found that as the aspect ratio of an interdigitated fuel cell decreased, the net power density increased as well [29]. Those experimental results have been built upon and reinterpreted to provide more insight and to serve at a motivation for the rest of the work. A PEMFC that can be operated under channel aspect ratio configurations of 50:1, called the low AR (5 cm channel length), 150:1, called the medium AR (15 cm channel length) and 250:1, called the high AR (25 cm channel length) through the use of isolated manifold exit ports was used in the experiment. An image of the flow field setup and picture of a bipolar plate can be found in Fig. 1. Manifolds were sized to be large enough to not contribute to pressure losses. "Outlet, High AR", "Outlet, Medium AR", and "Outlet, Low AR" were used for the high, medium and low aspect ratio conditions, respectively. The plates were machined out of 6061-T6 aluminum and were nickel coated for corrosion prevention. To run the cell under interdigitated conditions, repositionable 1 mm × 1 mm × 3 mm silicon plugs were used to seal off entrances and exits of cathode channels as shown in Fig. 1. Kapton ® tape was placed over unused portions of the cathode and anode MEA to prevent electrochemical reactions in the low and medium aspect ratio configurations. Plastic plugs were used to fill and block off manifold outlets that were not in use. The MEA consisted of SGL 10BC carbon GDL on both the anode and the cathode and a DuPont Nafion XL membrane with 27.5 μm thickness and 0.4 mg cm^{-2} platinum loading on both sides. Silicon gaskets were used to seal the MEA and cell compression was kept consistent throughout the testing process.

2.2. Testing parameters & statistical analysis

An Arbin Instruments® Fuel Cell Test Station was used to conduct the cell testing. It controlled the cell voltage, the cell current, the cell temperature and the feed gas conditions (temperature, humidity, flow rate). Cell temperature was monitored using k-type thermocouples and maintained via 4 cartridge heaters. Inlet pressure was measured using a Miljoco® gauge. All flow hardware was insulated to maintain gas temperatures. Polarization curves were conducted at two stoichiometries of 1.5 anode/2.0 cathode (called 1.5/2) and 2.0 anode/4.0 cathode (called 2/4). Three replications of each case were completed in random order. Polarization curves shown in the text are the average of the three replications. Galvanostatic control was used. Testing parameters used in the experiment can be found in Table 1.

Statistical analysis was completed on the experimental data using an analysis of variance (ANOVA) method to isolate the effect of key variables. The input variables were aspect ratio and stoi-

Table 1
Experimental testing parameters.

Parameter	Value
Cell temperature	70 °C
Gas temperatures	70 °C
Inlet humidity	85% RH
Current steps	1 A
Stoichiometries	1.5/2 and 2/4
Aspect ratios	250:1, 150:1 and 50:1

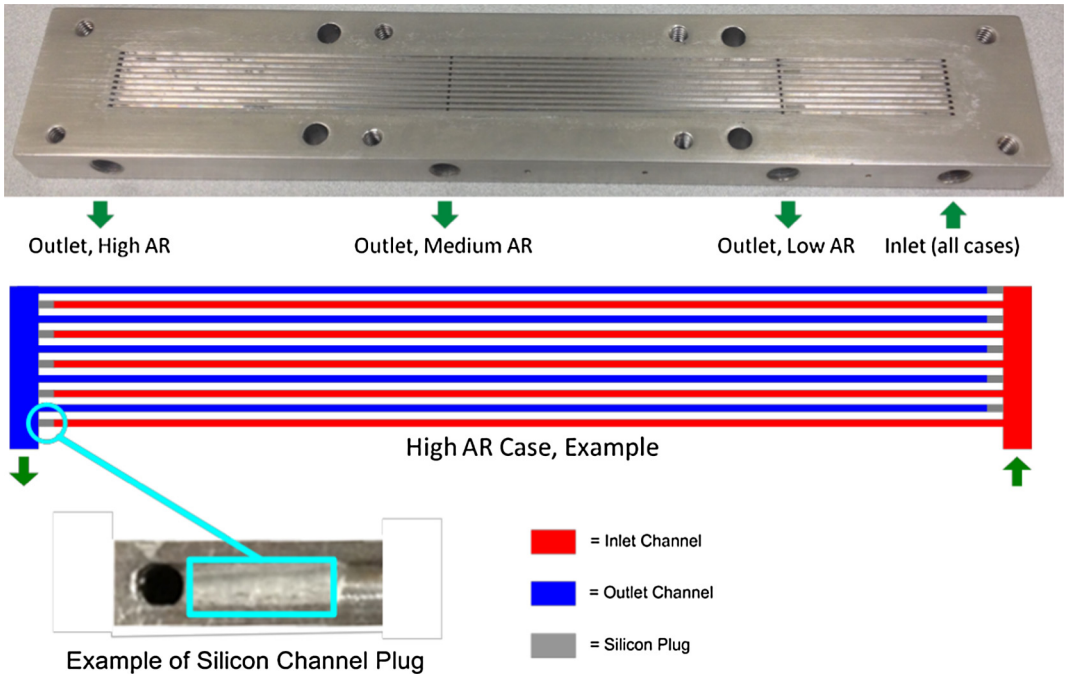

Fig. 1. Image of a bipolar plate of the fuel cell and silicon plugs used to induce interdigitated flow. Silicon plugs prevented flow into exit channels and out of entrance channels, causing cross flow. This method was used for each aspect ratio.

chiometry, with levels of high, medium & low aspect ratios, and 2/4 & 1.5/2 stoichiometries, respectively. The output variables were maximum cell power density (P_{max}) and limiting current density (j_L). For this experiment, limiting current density is the current density for which the corresponding steady state voltage drops below 0.05 V. ANOVA compares the variance of the data within each level of a condition with the variance of the data between levels of the condition. Using these variances, the total number of data points, and the number of levels, a measure of statistical significance is obtained. The critical p-value used for statistical significance for this ANOVA was 0.05.

3. Experimental results

The polarization trends for each aspect ratio are depicted in Fig. 2a and b. A portion of these results may be found in [29] in a different context, but here it has been reinterpreted, more data has been taken and it serves as a motivation for the work. After including parasitic pump losses, the voltage generally decreases at a given current density with increasing aspect ratio. The low aspect ratio cell performed the best over the entire range of current densities, while the high aspect ratio cell generally performed the worst. Even though the high aspect ratio cell generally performed the worst, it did exhibit less sensitivity to losses in the concentration region of the polarization curve compared to the medium aspect ratio cell. This affect was more pronounced in the 2/4 stoichiometry condition. This may indicate that the high aspect ratio cell experienced some better water removal characteristics from the very high pressure drop through the cell, compared to the medium aspect ratio case. The unsteady characteristic of the high and medium aspect ratio configurations at high current density in the 1.5/2 stoichiometry case indicates liquid water was a problem, supporting this theory.

System power, $\dot{E}_{sys}$, is compared by subtracting the required pumping power, $\dot{E}_{pump}$, from the cell power, $\dot{E}_{cell:}$

$$\dot{E}_{sys} = \dot{E}_{cell} - \dot{E}_{pump} \tag{1}$$

in units of milliwatts. Inlet cathode pumping pressure, p_{inlet}, changes with current density, so pumping power is determined by the non-isothermal compressor equation:

$$\dot{E}_{pump} = \frac{\dot{m}_{Air} C_p T}{\eta}\left(\left(\frac{p_{inlet}}{p_{atm}}\right)^{\frac{k-1}{k}} - 1\right) \tag{2}$$

where $\dot{m}_{Air}$ is the mass flow rate of reactant air, C_p is the specific heat of air (J kg^{-1} K^{-1}), T is the temperature of the air (K), η is the pump efficiency (~85%), p_{atm} is the atmospheric pressure and k is the specific heat ratio. Fig. 2c and d compares system power density for the interdigitated aspect ratio conditions versus current density. Overall, the low aspect ratio cell displays the highest performance while the medium and high aspect ratio configurations suffer from pressure loss in addition to the reduced power from liquid water and potential losses from uneven distribution of cross flow.

The ANOVA results are presented in Table 2. Both aspect ratio and stoichiometry input variables were found to have a statistically significant effect on cell maximum power and limiting current density. Interestingly, the interaction between stoichiometry and aspect ratio was found to be statistically significant for maximum power density but not limiting current density. This may be caused by the maximum power density's dependency on the multiplication of voltage and current density. The voltage at a given current density is dependent on environmental variables, such as inlet pressure or flow rate of reactants. Stoichiometry and aspect

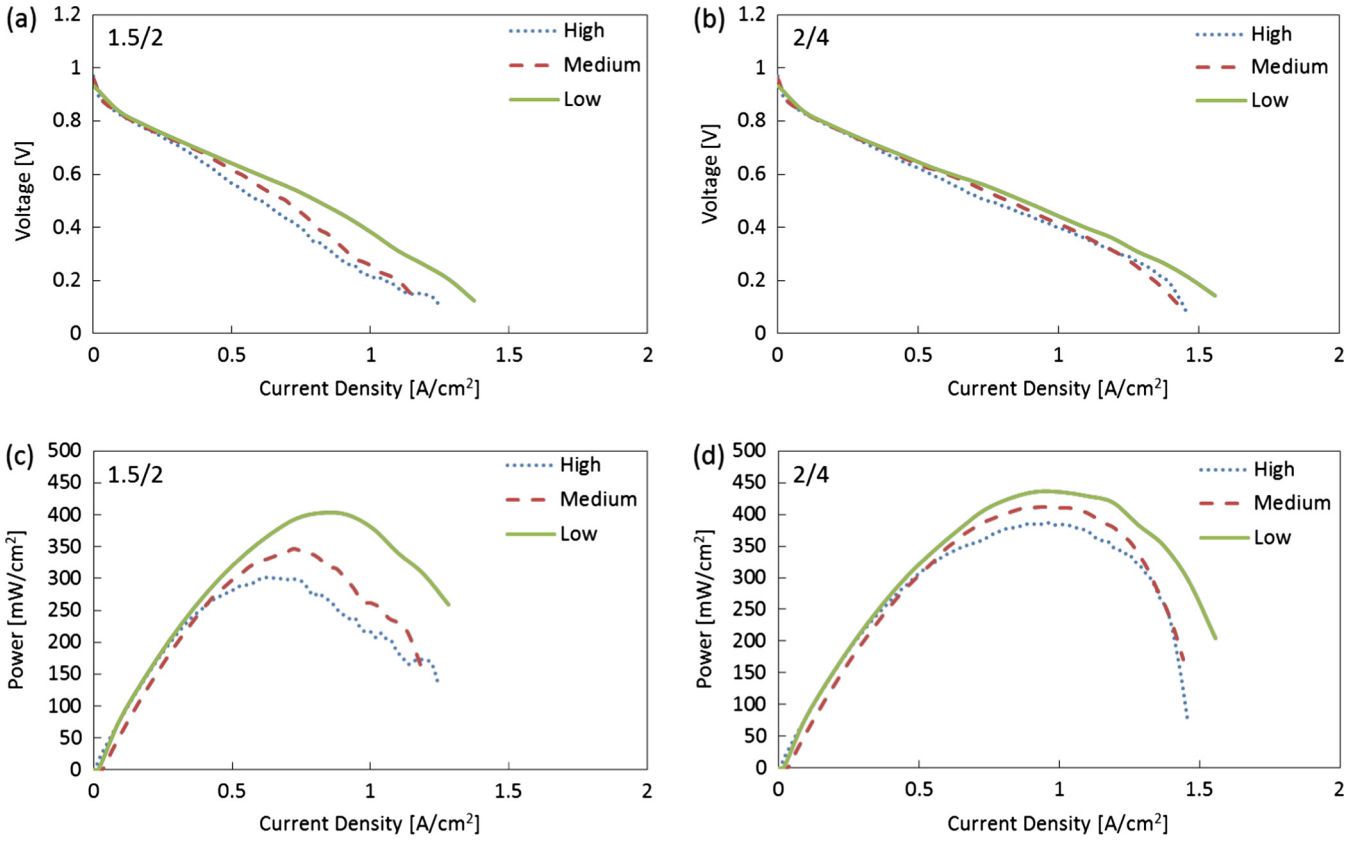

Fig. 2. The polarization curves for each aspect ratio, at (a) 1.5/2 and (b) 2/4 stoichiometries. Each polarization curve is the average of three separate runs. The system power curves for each aspect ratio, at (c) 1.5/2 and (d) 2/4 stoichiometries.

Table 2
ANOVA results. Given are the p-values for each input on each output. Outputs of interest are limiting current density, J_L, and maximum power, P_{max}, while inputs are stoichiometry and aspect ratio. The interaction between the two inputs was also examined. Statistically significant ($p < 0.05$) values are bolded.

	J_L	P_{max}
Stoichiometry	**4.05×10^{-7}**	**1.36×10^{-7}**
Aspect Ratio	**6.77×10^{-6}**	**3.62×10^{-7}**
Interaction	0.529	**0.0153**

ratio affect many of these environmental variables, and therefore vary the voltage. Since electrochemical effects tend to be nonlinear, the voltage response change may be non-proportional to the corresponding changes in environmental variables. This is carried through to the power calculation.

Given these interesting results, it is important to try and understand the cause of the performance degradation, so proper interdigitated flow field designs can account for the losses. The two potential causes of performance loss are liquid water accumulation in the cell and uneven distribution of cross flow. These will be explored to determine the relative contribution to performance degradation.

4. Neutron radiography

4.1. Processing

Neutron radiography was performed to determine whether water was a significant factor in the performance differences between the high and low aspect ratio designs. Neutron radiography produces an image of the internal structure of the fuel cell based on the attenuation of neutrons through the fuel cell. Neutron attenuation is not directly related to the density of the material, but is dependent on the neutron cross section of those materials. Metals, particularly aluminum, can have a relatively low neutron cross section, meaning radiographs can see the internal structure. Hydrogen, and by extension water, has a relatively high neutron cross section, meaning water can be seen easily on neutron radiographs. Beam attenuation in neutron imaging is governed by the Lambert-Beer Law

$$I = I_0 e^{-\sum[\Sigma_i x_i]} \tag{3}$$

where I is the transmitted neutron flux, I_0 is the initial neutron flux, and Σ_i and x_i are the macroscopic cross section (neutron attenuation coefficient) and thickness of imaged material layer i, respectively. The amount of water present in-situ in the fuel cell can be determined by comparing the transmitted fluxes of a dry fuel cell which has been purged, and a fuel cell that has run and accumulated water. A dry, purged fuel cell, where subscript D means *Dry*, and a wet fuel cell, where subscript W means *Water*, would have Lambert-Beer Laws of

$$I_{Dry} = I_0 e^{-\Sigma_D x_D} \tag{4}$$

$$I_{wet} = I_0 e^{-[\Sigma_D x_D + \Sigma_w x_w]} \tag{5}$$

Using a dry shot and a wet shot, the relative intensity of the water can be determined. Rearranging terms gives

$$\Sigma_w x_w = -\ln\left(\frac{I_{wet}}{I_{dry}}\right) \tag{6}$$

This gives the relative thickness of the water at each point in the radiograph. All images were normalized using a point from the image which did not contain water. This was done to minimize the effect of possible beam intensity fluctuations.

4.2. Testing parameters

All imaging was performed in Bay 3 at the McClellan Nuclear Radiation Center, which is an experimental TRIGA reactor rated for up to 2 MW of steady state power. The bay is at a 30° angle from horizon, and has a thermal neutron flux of 4.3×10^6 n cm^{-2} - s^{-1}. The scintillation screen and image resolution is 100 μm. The beam aperture is 1.54 in. and the beam line has an L/D ratio of 175. The camera used to capture images is an Apogee Alta cooled to −40 °C, with an E2V back illuminated CCD40-42. All neutron images, also known as radiographs, were collected by averaging two pictures taken with 40 s of beam exposure time each. Three separate radiographs were collected for each aspect ratio and operating condition imaged.

The imaging used the same fuel cell set up as was used in the testing. The testing parameters used may be found in Table 3. Due to time constraints, only high and low aspect ratio fuel cell designs were imaged. To isolate the cathode flow field liquid water, relative humidity on the anode was set to 50% to minimize anode flooding. This may have an effect on the liquid water back diffusion, but the trends on water accumulation in the high and low aspect ratio will still be similar. All other operational parameters were the same as during testing. Images were captured at two current densities to get a better sense of the effect of water generation rates on the water distribution - a low current density which provides a low water generation rate and a current density at which a fuel cell might be typically operated.

4.3. Imaging results

Sample radiographs of both the high and low aspect ratio cells, at two different operational conditions can be found in Fig. 3. Only the flow field between the silicon plugs used in the channels is shown, as this is where flow phenomena occur. On the high aspect ratio cell, the artifacts at approximately 20% and 60% of the way down the length of the cell are the low and medium AR manifolds built into the bipolar plates. These were blocked to prevent flow between channels, but the edges of the manifold can still show up on the neutron image. Water slugs can be seen blocking channels as the yellow and red sections in the channels.

The water distribution trends down the length of the flow field can be found in Fig. 4, as the average across the width of the cell. Comparing the low (Fig. 4a) and high (Fig. 4b) aspect ratio overall trends, the low aspect ratio flow field tended to have an even distribution of water down the length of the cell, while the high aspect ratio flow field tended to have water buildup toward the outlet of the cell. The low aspect ratio experienced a minor buildup in liquid water near the outlet of the cell, in comparison. Upon examination of the raw radiographs, the increase in the saturation level of the high aspect ratio cell was due to water slugs found in entrance channels that build up on the outlet end of the cell. This position will multiply the effect of the water slug on performance, as it prevents cross flow at the outlet end of the fuel cell. The increase in the saturation of the low aspect ratio fuel cell may be

Table 3
Imaging testing parameters.

Parameter	Value
Cell temperature	70 °C
Gas Temperatures	70 °C
Cathode inlet humidity	85% RH
Anode inlet humidity	50% RH
Current densities	0.2 A cm^{-2} and 0.6 A cm^{-2}
Stoichiometries	1.5/2 and 2/4
Aspect ratios	250:1 and 50:1

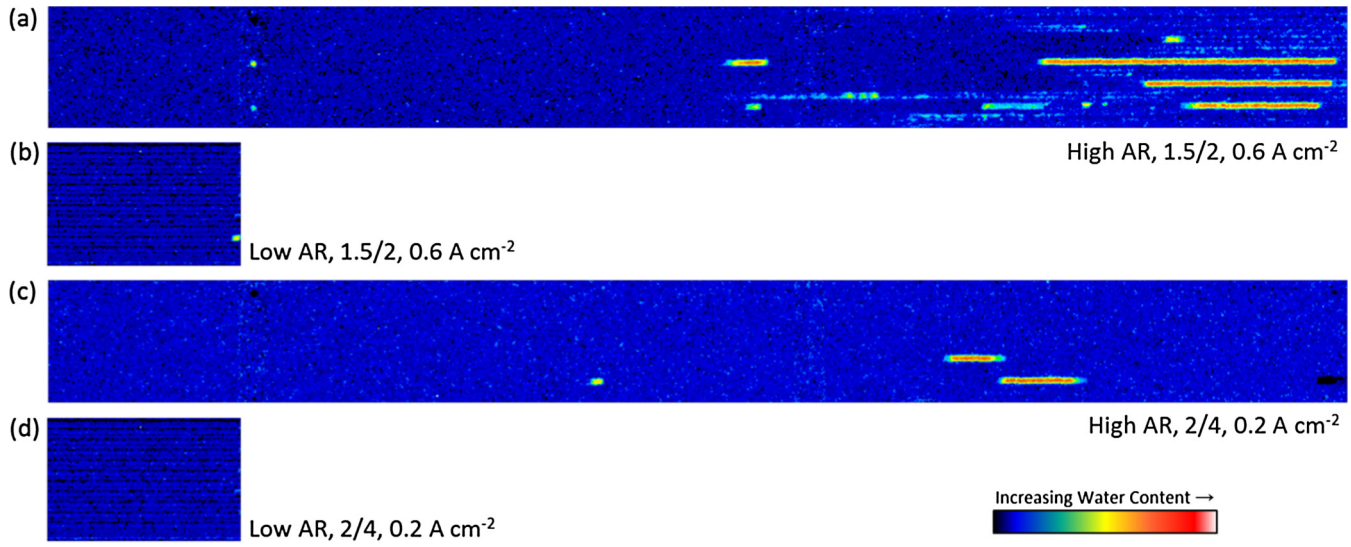

Fig. 3. Sample images from neutron radiography, of (a) the high aspect ratio, 1.5/2 stoichiometry, at 0.6 A cm^{-2}, (b) low aspect ratio, 1.5/2 stoichiometry, at 0.6 A cm^{-2}, (c) high aspect ratio, 2/4 stoichiometry, at 0.2 A cm^{-2}, and (d) low aspect ratio, 2/4 stoichiometry, at 0.2 A cm^{-2}. The color bar in the lower left shows the thickness of water increases from black/blue (little to no water) to red/white (saturation). The left side of the images is the inlet and the right side is the outlet. (For interpretation of the references to color in this figure legend, the reader is referred to the web version of this article.)

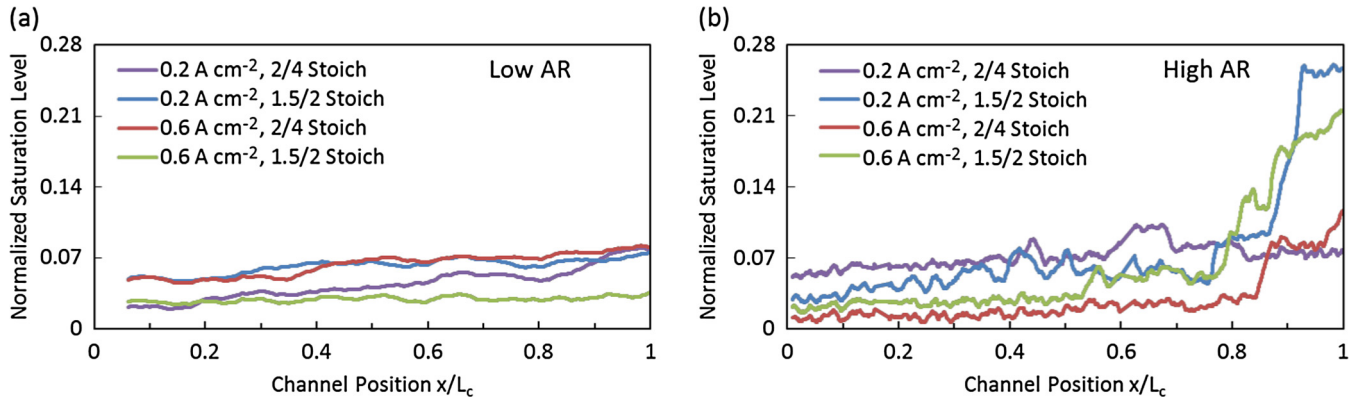

Fig. 4. The distribution of water down the length of the fuel cell, averaged across the width of the flow field for (a) the low aspect ratio and (b) the high aspect ratio. The x-axis is the channel position from inlet, at 0, to outlet, at 1. The y-axis is the average saturation level of water for that point in the channel position, across the entire width of the cell.

due to the increasing humidity of the cathode reactants as they flow through the cell.

The high aspect ratio cell had the most liquid water in the 0.2 A cm^{-2}, 1.5/2 stoichiometry condition. This condition had the lowest reactant flow rate through the fuel cell, so the cell may have had difficulty removing water that built up in the GDL. The 0.2 A cm^{-2}, 2/4 stoichiometry condition had the most consistent water accumulation down the length of the cell, which could be explained by the combination of high reactant flow rates and the low water production rate. The low aspect ratio cell experienced comparatively minor differences in the level of water accumulation between the various operating conditions.

This water distribution data corroborates and clarifies the findings from the experimental results. The difference in liquid water accumulation between the high and low aspect ratio flow fields seems to indicate that liquid water buildup in the flow field plays a major part in performance degradation with increasing aspect ratio. The high aspect ratio fuel cell has water concentrated in entrance channels at the outlet side of the flow field, potentially exacerbating performance loss affects as this renders portions of the cell inaccessible to reactants. The performance differences observed in the experiment between high and low aspect ratio flow fields at high current densities match the increase in water buildup in the high aspect ratio flow field at high current density, lending further support to the liquid water theory. The performance degradation due to liquid water cannot be directly quantified, so the performance degradation due to uneven distribution of cross flow must first be determined before the relative attribution of affect magnitude is made.

5. Simulation formulation

5.1. Geometry and assumptions

For computational simplicity, a differential, half channel portion of the PEMFC was modeled using COMSOL Multiphysics with the Batteries and Fuel Cells module, which can be seen in Fig. 5. The model is single phase. This is important, as the model is meant to only capture performance effects due to uneven flow distribution; the water affects are identified from the neutron radiography. This effect will be compared to the losses determined from the

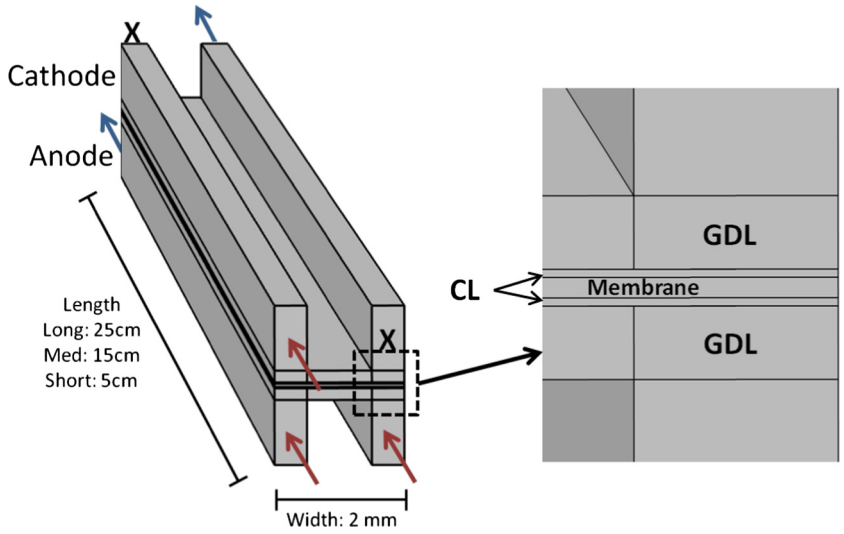

Fig. 5. Flow domains of the model. Red arrows indicate inlets to the half channels, while blue arrows indicate outlets of the half channels. The X indicates half channels which are blocked off. The anode has another outlet at the end of the right half channel, but this is behind the model. (For interpretation of the references to color in this figure legend, the reader is referred to the web version of this article.)

experimental portion of the work. Any experimental losses not attributable to the single phase model are due to the liquid water identified in the neutron radiography. Half channel models have been used by other groups and are a simple, reliable way of minimizing computation time [1,30,31]. The differential model includes both anode and the cathode portions of the PEMFC. As a representative portion of an interdigitated cell, the differential model must have both an entrance and an exit channel on the cathode. The boundaries of the model are halfway through the entrance and exit channels, and have symmetry conditions applied to simulate full channel gas movement. On the anode side, both half-channels are in parallel. The model is isothermal, steady state, single phase, with ideal gases and no gas or water crossover or contact resistance.

5.2. Governing equations and boundary conditions

Compressible flow conservation laws were applied to the model. Relevant laws in the model included the continuity equation, and momentum conservation in channels. Flow in porous media was handled using the Brinkman modification to the Darcy equation [32]. Charge and species conservation equations were also applied.

All walls had no-slip boundary conditions. The inlet and outlet conditions were set to be laminar. The inlet velocity was set to be the same as the experiment at the maximum power point. The exit was set to atmospheric pressure. Velocity field and pressure distributions from the Navier-Stokes equation and the Darcy-Brinkman equation were set to be equal across CL-GDL and GDL-channel boundaries.

The anode overpotential was calculated using the linearized Butler-Volmer equation, as the overpotentials from the anode side are relatively small. The cathode overpotential was calculated using the Tafel equation, as the overpotentials from the cathode are relatively large. The average current density was calculated by averaging the local current density over the whole area of the cell.

5.3. Parameter selection

The PEMFC operating conditions and material properties listed in Tables 4 and 5 were chosen to reflect the components and materials used in the experiment. The porosity for GDL under compression was accounted for by approximating the volumetric ratio change of the compressed GDL from the uncompressed GDL. In this study, ε_{comp} was 0.73. The permeability of the compressed GDL was then matched from data published by Gostick et al. [33].

The lengths of the channels, L, were set to be the same as the lengths of the PEMFC design used for the experiment. These lengths resulted in aspect ratios of 50:1, 150:1 and 250:1. The inlet

Table 4
PEMFC Model parameters that are constant across all conditions.

Variable	Value	Description
T_{cell} (°C)	70	Cell temperature
P_{exit} (Pa)	0	Outlet pressure (gage)
ε_{gdl}	0.82	Porosity of GDL
κ_{gdl} (m^2)	3.65e−11	Permeability of GDL [34] and [35]
ε_{cl}	0.35	Porosity of CL [36]
v_l	0.3	Electrolyte volume fraction in the CL [36]
κ_{cl} (m^2)	6e−12	Permeability of CL [37]
V_ratio	0.667	Vol. ratio change compressed GDL
ε_{comp}	0.73	Porosity of compressed GDL
κ_{cl} (m^2)	7e−12	Permeability of compressed GDL [33]
t_{gdl} (μm)	180	Thickness of GDL
t_{cl} (μm)	20	Thickness of CL
t_{mem} (μm)	50	Thickness of membrane
w_{ch} (mm)	1	Channel width
w_{land} (mm)	1	Land width
d (mm)	1	Channel depth
T_{dew} (°C)	65	Gas dew point
V (V)	0.72	Voltage of the cell
σ_{mem} (S/m)	7	Conductivity of membrane [38]
σ_{gdl} (S/m)	250	Conductivity GDL
A_s (1/m)	10^8	Active specific surface area
$\alpha_{cathode}$	0.5	Cathodic transfer coefficient [39]
α_{anode}	0.5	Anodic transfer coefficient [39]
A_c (mV)	−70	Cathodic Tafel Slope [40]

Table 5
PEMFC Model parameters that are condition dependent for the 2/4 stoichiometry condition.

Variable	Short	Medium	Long	Description
$U_{in,cathode}$ (m/s)	1.23	2.36	5.94	Inlet velocity on cathode
$U_{in,anode}$ (m/s)	0.2	0.38	0.96	Inlet velocity on anode
L (cm)	5	15	25	Channel length

velocities, $U_{in,anode}$ and $U_{in,cathode}$, were calculated based on the flow rate of each reactant gas stream at the current density of the maximum power density, for both stoichiometries of the PEMFC used in the experimental portion of the work.

6. Simulation results

6.1. Pressure

A comparison of the measured pressure drops across the cell to the simulated pressure drops is found in Table 6. Pressure trends increase with higher aspect ratios due to head loss from channel walls and higher flow rates needed to maintain the same stoichiometric values. The simulated pressures are lower than the pressure measured in the experimental cell. Since the simulation was meant to strictly examine the effect of uneven distribution of cross flow, the differences are most likely due to liquid water build up in the experimental cell, and pressure losses from flow in gas lines and the manifolds.

Table 6
Comparison of numerical and experimental pressure drops through the cell, in kPa. The experimental pressure is the pressure through the cell at 0.6 A/cm^2. Note: The minimum, non-zero, pressure measurable using the experimental setup is 0.689 kPa.

	Numerical		Experimental	
	2/4 Stoichiometry	1.5/2 Stoichiometry	2/4 Stoichiometry	1.5/2 Stoichiometry
Low	0.298	0.144	1.896	0.689
Medium	1.433	0.468	1.724	0.689
High	4.778	1.398	5.860	4.137

The pressure trends for each aspect ratio simulated at the 2/4 stoichiometry can be found in Fig. 6. Fig. 6a–c show the pressure in the channels. The entrance channels are labeled High Pressure and the exit channels are labeled Low Pressure. In the high aspect ratio cell, the pressures of the entrance and exit channels are so similar as to essentially overlap for approximately 50% of the cell length. The parabolic nature of these curves may be due to the balance between head loss down the length of the cell and pressure from cross flow through the GDL. The head loss due to flow in channels is the same for both entrance and exit channels, so given enough distance the channels will equalize pressure. This persists until the equilibrium is disturbed by the outlet in the exit channel. These results are corroborated by previous numerical interdigitated studies, such as Arato et al. [14].

Fig. 6d overlays the deviation of the pressure differential between channels, ΔP_x, at a length down the channel, x, from the

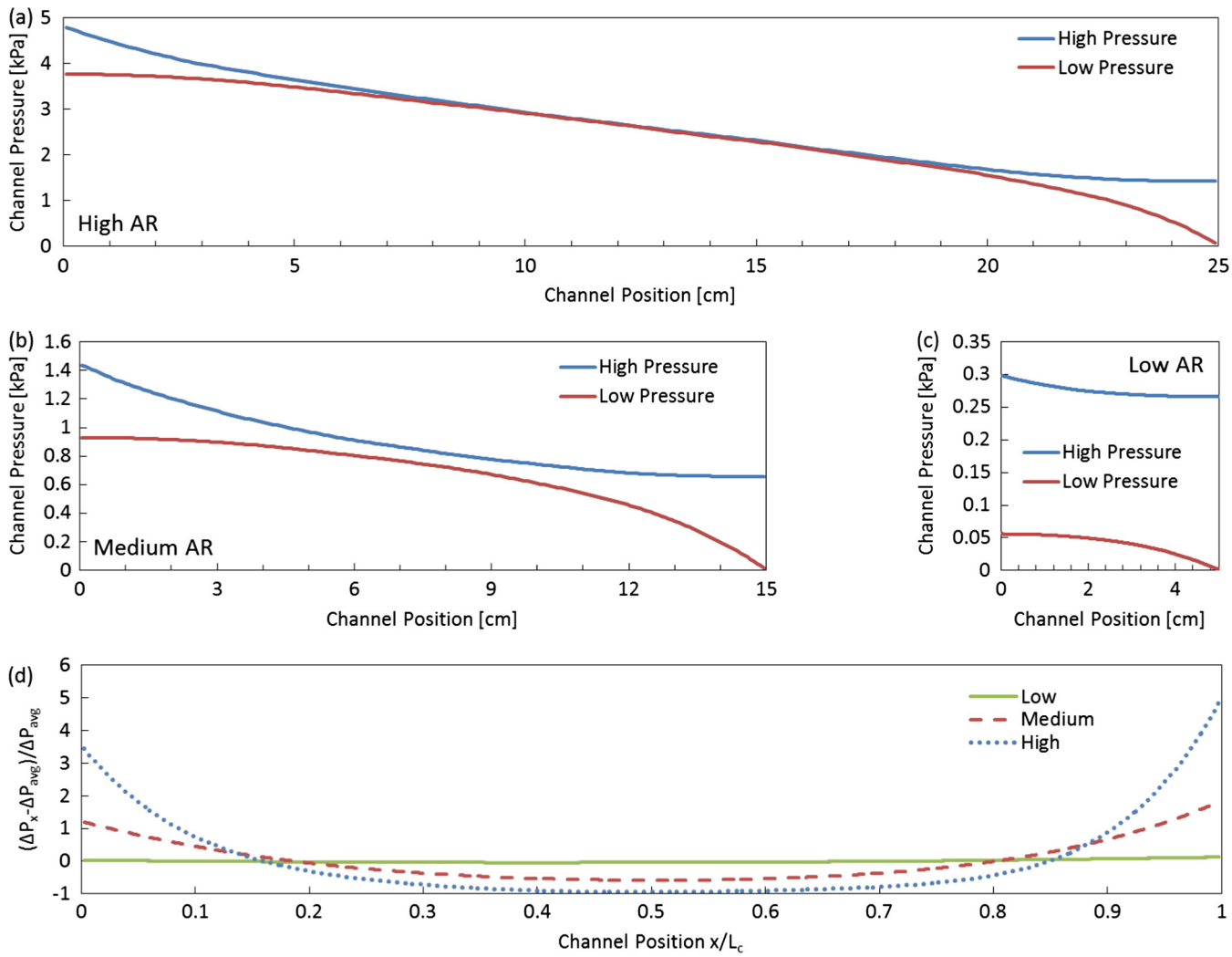

Fig. 6. Plot of pressure distributions in entrance and exit channels in the (a) high aspect ratio cell, (b) medium aspect ratio cell and (c) low aspect ratio cell. (d) The deviation from the average pressure differential at normalized position in the channel. All data taken for the 2/4 stoichiometry case.

average pressure differential between channels, ΔP_{avg}, for each channel length, against the dimensionless position down the length of the channel x/L_c. Both the high aspect ratio cell and medium aspect ratio cell maintain their parabolic shape, while the low aspect ratio cell is more even down its length.

Pressure differential between channels is directly relatable to cross flow rate, as has been previously shown [41]. By relating the pressure differential to cross flow rates, it becomes clear that cross flow rate is unevenly distributed down the length of the cell due to the variations is pressure differences. In the high aspect ratio cell, cross flow rate is concentrated at the ends of the cell, while the center experiences significantly lower than average cross flow rates. The medium aspect ratio cell also experiences uneven distribution of cross flow down the length of the cell, but to a lesser extent. The low aspect ratio cell has relatively even cross flow rates.

6.2. Current density

The local current density in the membrane becomes less evenly distributed with increasing aspect ratio. This can be seen in Fig. 7a–c. Both the medium and the high aspect ratio cells exhibit reduced current density production in the middle of the flow field, and elevated current densities at the inlet and outlet ends of the flow field. Compared to the other cases, the low aspect ratio case has fairly evenly distributed current density down the length of the cell. There is a small but noticeable reduction in current density near the end of the cell, due to concentration loss down the cell, as reactant gets used, reducing the rate of diffusion. The low aspect ratio cell does not have a significant increase in cross flow at the outlet of the cell, so does not have an increase in current density production to counteract the concentration losses. This concentration loss effect is also observable over lands in the cell. As the reactant flows through the GDL, some gas is reacted by the catalyst layer. The remaining reactants in the cross flow stream have a lower concentration, increasing concentration losses.

The relationship between average current density production across the width of the cell and position along the length is shown in Fig. 7d. The medium and high aspect ratios have less even current density production than the low aspect ratio. The medium and high aspect ratio designs underperform the low aspect ratio design for approximately two-thirds of their length in middle, but outperform the low aspect ratio at the inlet and outlet. This is due to the increased cross flow rates at the inlet and outlet of the fuel cell.

The uneven distribution of current density in the membrane leads to a decrease in the overall average current density production, with increasing aspect ratio. The gain in current density caused by high cross flow areas is less than the loss in current density caused by low cross flow areas. This results in small areas of high cross flow & current density, such as the inlet and outlet of the medium or high aspect ratios, and large areas of low cross flow & current density, such as the middle of the medium or high aspect ratio cells. Increasing the aspect ratio of the cell would cause the average cell current density to decrease, as larger and larger proportions of the cell support low cross flow. These low cross flow

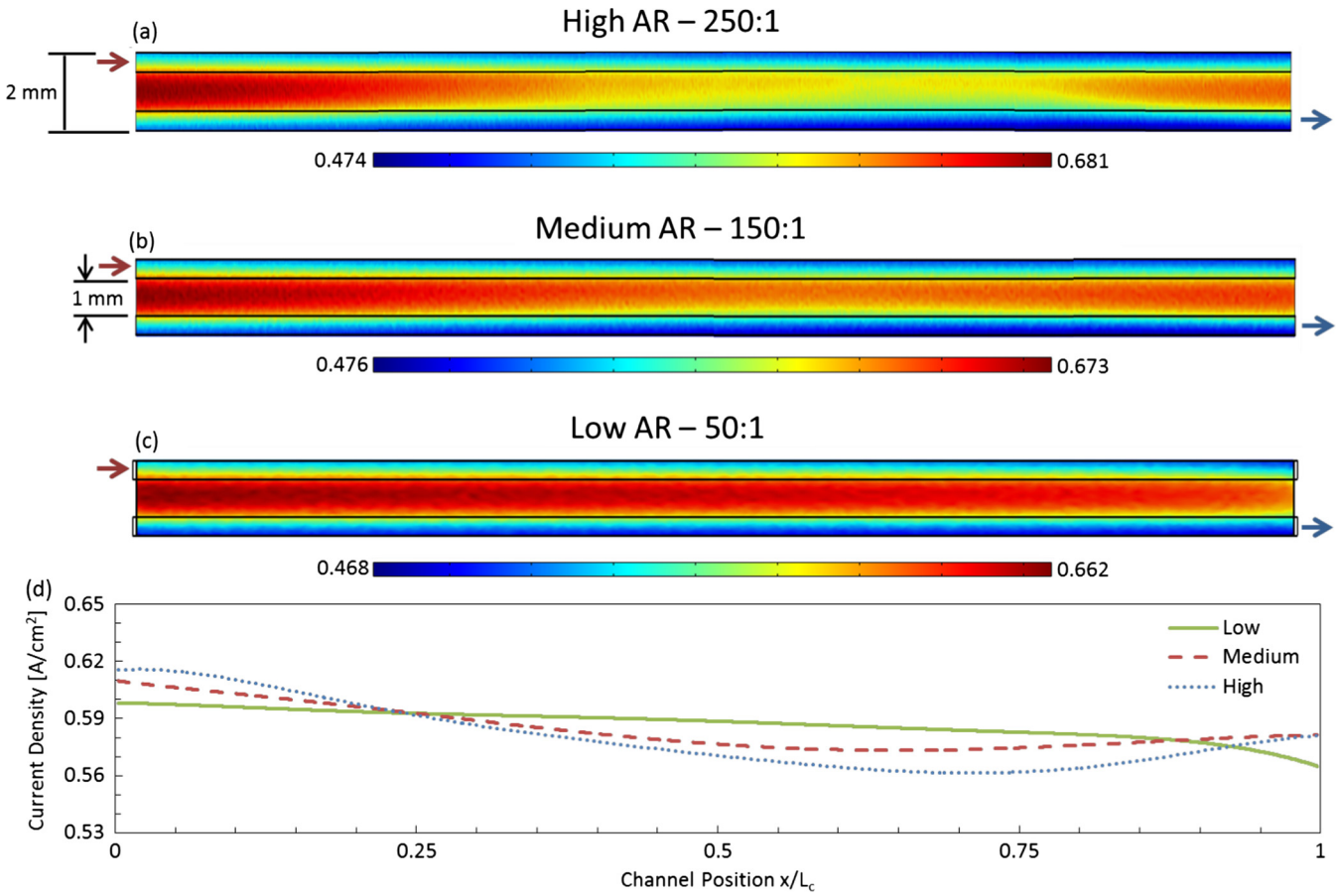

Fig. 7. The current density distribution halfway through the membrane for (a) high aspect ratio (b) medium aspect ratio and (c) low aspect ratio. Not to scale, each aspect ratio shown has been blown up to benefit visualization. (d) Current density production at normalized position down the cell. Simulation performed for a cell voltage of 0.72 V. All data taken for the 2/4 stoichiometry case.

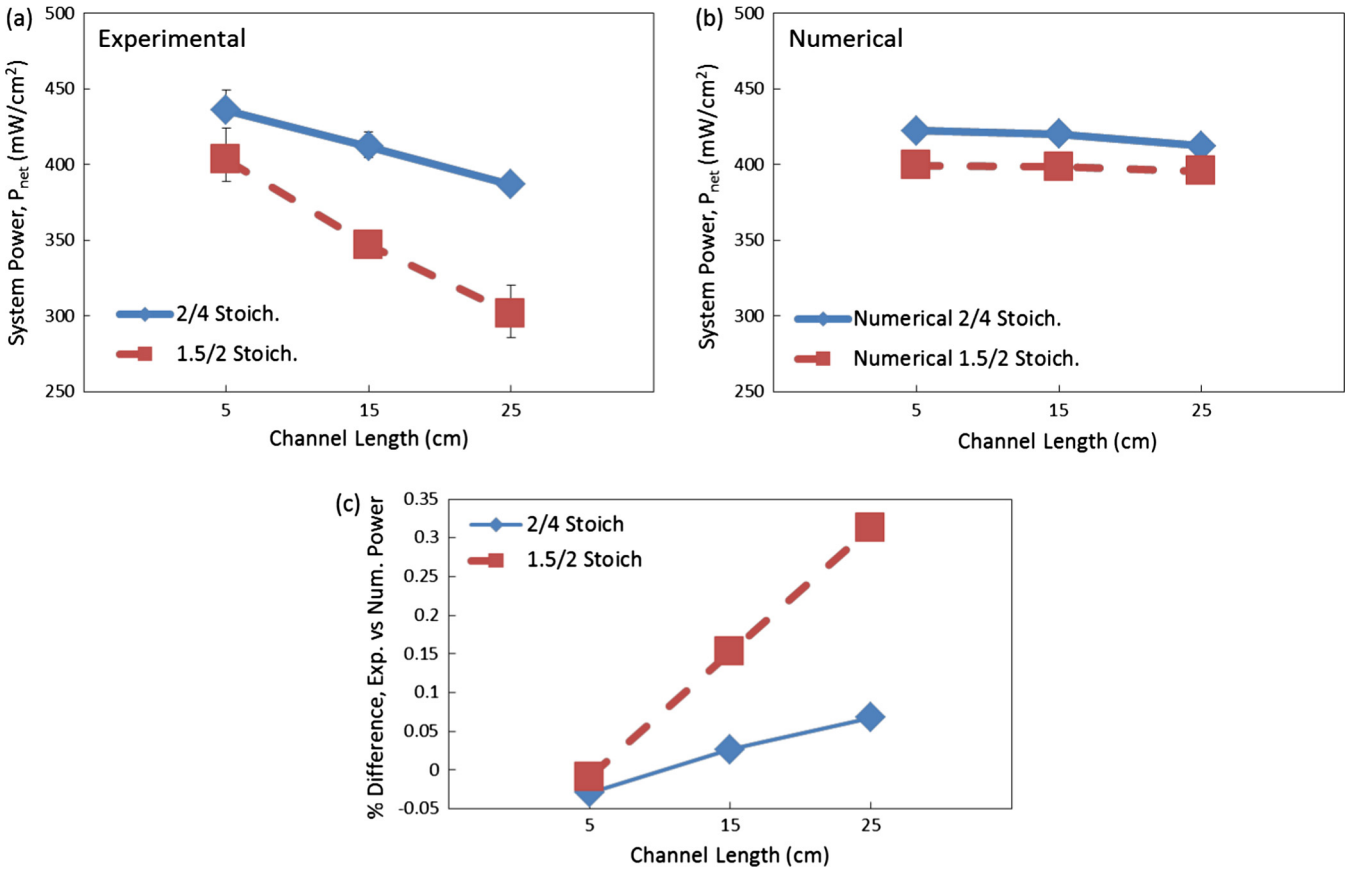

Fig. 8. Net power density, after subtracting pumping power, of the PEMFC at each length at both 2/4 and 1.5/2 stoichiometries for (a) the experimental results, (b) the numerical simulation and (c) a percentage difference in the power between the experiment and simulation.

areas can be best considered as being sections of parallel flow field behavior within the interdigitated flow field. The reactant gases are reliant on diffusion rather than convection to get reactant to the catalyst layer under the lands, increasing the required diffusion length for these portions of the cell.

6.3. Power density comparisons

The simulation results and the experimental testing at the max power point are displayed in Fig. 8. By comparing the results of the experiment and the simulation, the relative effect of the uneven distribution of cross flow on performance losses may be determined, and the relative effect of liquid water can be attributed. Both experimental and numerical data show decreasing trends in power density due to increasing aspect ratio. In the simulation, at 2/4 stoichiometry, the medium aspect ratio cell has 0.6% less power than the low aspect ratio cell, while the high aspect ratio cell loses 2.5% power compared to the low aspect ratio cell. At 1.5/2 stoichiometry, the differences become even smaller, losing less than 1% of net power density each. In the experimental data, on the other hand, at the 2/4 stoichiometry, the medium aspect ratio cell has 5.5% less power than the low aspect ratio cell, and the high aspect ratio cell has 11% less power. At the 1.5/2 stoichiometry, the power loss is even more noticeable, at 14% and 25% respectively.

The experimental data shows a larger reduction in performance with increasing aspect ratio compared to the simulation. In Fig. 8c, the percentage difference between the experimental and the simulation results can be seen to increase with increasing aspect ratio. This indicates that the main cause of power density losses in the cell is probably not the uneven cross flow distribution, but instead the liquid water in the flow field identified in the neutron imaging. It is interesting to note that the simulation and experimental data have opposite trends when it comes to stoichiometry. The effect of power loss is more pronounced in the simulation at 2/4 stoichiometry, whereas in the experimental data, the power loss is far more pronounced at 1.5/2 stoichiometry. This further supports the idea that liquid water build up is the main cause of power degradation, as at higher stoichiometries, more reactant is flowing through the cell, increasing the pressure. The lower pressure of 1.5/2 stoichiometry is less able to push water out of the GDL and channels, causing greater performance losses.

7. Conclusions

This study examined the relationship between decreasing channel aspect ratio and performance improvement in interdigitated flow field PEMFCs. The motivating experiment showed that low aspect ratio interdigitated flow fields tend to outperform high aspect ratio designs. A statistical analysis found that there was a statistically significant interaction between channel aspect ratio and the stoichiometry for the maximum power density. Neutron radiography determined there was increased water accumulation in the high aspect ratio flow field compared to the low aspect ratio flow field. The neutron radiography further showed an increase in water content at higher current densities, which corresponded to the greater performance losses seen in the experiment. These observations indicate that liquid water removal was most likely the major cause of performance improvement with decreasing aspect ratio, but the change in the distribution of cross flow had

to be examined as well for confirmation. A liquid water-free simulation examined the impact of uneven distribution of cross flow on performance. The performance loss due to uneven cross flow was notably less than the performance loss with increasing aspect ratio measured in the experiment, indicating that liquid water was probably the major cause of performance loss. Designers of interdigitated PEMFC, including flow-field switching designs, should take into account these performance issues and explore using a lower aspect ratio layout if possible and pursuing either parallel designs or a liquid water elimination system when higher aspect ratios are necessary.

Acknowledgements

We would like to thank the Korea Institute of Energy Research for providing support for this work.

References

[1] He W, Yi JS, Van Nguyen T. Two-phase flow model of the cathode of PEM fuel cells using interdigitated flow fields. AIChE J 2000;46:2053–64. http://dx.doi.org/10.1002/aic.690461016.
[2] Nguyen TV. A gas distributor design for proton exchange membrane fuel cells. J Electrochem Soc 1996;143:L103–5. http://dx.doi.org/10.1149/1.1836666.
[3] Wood Iii DL, Yi JS, Nguyen TV. Effect of direct liquid water injection and interdigitated flow field on the performance of proton exchange membrane fuel cells. Electrochim Acta 1998;43:3795–809. http://dx.doi.org/10.1016/S0013-4686(98)00139-X.
[4] Bachman J, Santamaria A, Tang H-Y, Park JW. Investigation of polymer electrolyte membrane fuel cell parallel flow field with induced cross flow. J Power Sources 2012;198:143–8.
[5] Tong S, Bachman JC, Santamaria A, Park JW. Experimental investigation on a polymer electrolyte membrane fuel cell (PEMFC) parallel flow field design with external two-valve regulation on cathode channels. J Power Sources 2013;242:195–201. http://dx.doi.org/10.1016/j.jpowsour.2013.05.018.
[6] Ramiar A, Mahmoudi AH, Esmaili Q, Abdollahzadeh M. Influence of cathode flow pulsation on performance of proton exchange membrane fuel cell with interdigitated gas distributors. Energy 2016;94:206–17. http://dx.doi.org/10.1016/j.energy.2015.10.110.
[7] Heidary H, Kermani MJ, Dabir B. Influences of bipolar plate channel blockages on PEM fuel cell performances. Energy Convers Manage 2016;124:51–60. http://dx.doi.org/10.1016/j.enconman.2016.06.043.
[8] Taira H, Liu H. In-situ measurements of GDL effective permeability and underland cross-flow in a PEM fuel cell. Int J Hydrogen Energy 2012;37:1–6. http://dx.doi.org/10.1016/j.ijhydene.2012.03.030.
[9] Santamaria AD, Becton MK, Cooper NJ, Weber AZ, Park JW. Effect of cross-flow on PEFC liquid-water distribution: an in-situ high-resolution neutron radiography study. J Power Sources 2015;293:162–9. http://dx.doi.org/10.1016/j.jpowsour.2015.05.016.
[10] Chiu H-C, Jang J-H, Yan W-M, Li H-Y, Liao C-C. A three-dimensional modeling of transport phenomena of proton exchange membrane fuel cells with various flow fields. Appl Energy 2012;96:359–70. http://dx.doi.org/10.1016/j.apenergy.2012.02.060.
[11] Wu H, Berg P, Li X. Steady and unsteady 3D non-isothermal modeling of PEM fuel cells with the effect of non-equilibrium phase transfer. Appl Energy 2010;87:2778–84. http://dx.doi.org/10.1016/j.apenergy.2009.06.024.
[12] Wang XD, Yan WM, Duan YY, Weng FB, Jung G Bin, Lee CY. Numerical study on channel size effect for proton exchange membrane fuel cell with serpentine flow field. Energy Convers Manage 2010;51:959–68. http://dx.doi.org/10.1016/j.enconman.2009.11.03.
[13] Kanezaki T, Li X, Baschuk JJ. Cross-leakage flow between adjacent flow channels in PEM fuel cells. J Power Sources 2006;162:415–25. http://dx.doi.org/10.1016/j.jpowsour.2006.07.023.
[14] Arato E, Pinna M, Costa P. Gas-phase mass-transfer resistance at PEMFC electrodes: Part 2. Effects of the flow geometry and the related pressure field. J Power Sources 2006;158:206–12. http://dx.doi.org/10.1016/j.jpowsour.2006.01.050.
[15] Grujicic M, Zhao CL, Chittajallu KM, Ochterbeck JM. Cathode and interdigitated air distributor geometry optimization in polymer electrolyte membrane (PEM) fuel cells. Mater Sci Eng, B 2004;108:241–52. http://dx.doi.org/10.1016/j.mseb.2004.01.005.
[16] khazaee I, Sabadbafan H. Effect of humidity content and direction of the flow of reactant gases on water management in the 4-serpentine and 1-serpentine flow channel in a PEM (proton exchange membrane) fuel cell. Energy 2016;101:252–65. http://dx.doi.org/10.1016/j.energy.2016.02.02.
[17] Mahmoudi AH, Ramiar A, Esmaili Q. Effect of inhomogeneous compression of gas diffusion layer on the performance of PEMFC with interdigitated flow field. Energy Convers Manage 2016;110:78–89. http://dx.doi.org/10.1016/j.enconman.2015.12.012.
[18] Owejan JP, Gagliardo JJ, Sergi JM, Kandlikar SG, Trabold Ta. Water management studies in PEM fuel cells, Part I: fuel cell design and in situ water distributions. Int J Hydrogen Energy 2009;34:3436–44. http://dx.doi.org/10.1016/j.ijhydene.2008.12.10.
[19] Iranzo A, Boillat P, Biesdorf J, Tapia E, Salva A, Guerra J. Liquid water preferential accumulation in channels of PEM fuel cells with multiple serpentine flow fields. Int J Hydrogen Energy 2014;39:15687–95. http://dx.doi.org/10.1016/j.ijhydene.2014.07.101.
[20] Turhan A, Kim S, Hatzell M, Mench MM. Impact of channel wall hydrophobicity on through-plane water distribution and flooding behavior in a polymer electrolyte fuel cell. Electrochim Acta 2010;55:2734–45. http://dx.doi.org/10.1016/j.electacta.2009.11.095.
[21] Shimpalee S, Beuscher U, Van Zee JW. Analysis of GDL flooding effects on PEMFC performance. Electrochim Acta 2007;52:6748–54. http://dx.doi.org/10.1016/j.electacta.2007.04.115.
[22] Spernjak D, Prasad AK, Advani SG. Experimental investigation of liquid water formation and transport in a transparent single-serpentine PEM fuel cell. J Power Sources 2007;170:334–44. http://dx.doi.org/10.1016/j.jpowsour.2007.04.020.
[23] Spernjak D, Prasad AK, Advani SG. In situ comparison of water content and dynamics in parallel, single-serpentine, and interdigitated flow fields of polymer electrolyte membrane fuel cells. J Power Sources 2010;195:3553–68. http://dx.doi.org/10.1016/j.jpowsour.2009.12.031.
[24] Owejan JP, Trabold TA, Jacobson DL, Baker DR, Hussey DS, Arif M. In situ investigation of water transport in an operating PEM fuel cell using neutron radiography: Part 2 – transient water accumulation in an interdigitated cathode flow field. Int J Heat Mass Transf 2006;49:4721–31.
[25] Hickner Ma, Siegel NP, Chen KS, Hussey DS, Jacobson DL, Arif M. In situ high-resolution neutron radiography of cross-sectional liquid water profiles in proton exchange membrane fuel cells. J Electrochem Soc 2008;155:B427. http://dx.doi.org/10.1149/1.282628.
[26] Wang X-D, Duan Y-Y, Yan W-M, Peng X-F. Effects of flow channel geometry on cell performance for PEM fuel cells with parallel and interdigitated flow fields. Electrochim Acta 2008;53:5334–43. http://dx.doi.org/10.1016/j.electacta.2008.02.095.
[27] Bachman J, Charvet M, Santamaria A, Tang H-Y, Park JW, Walker R. Experimental investigation of the effect of channel length on performance and water accumulation in a PEMFC parallel flow field. Int J Hydrogen Energy 2012;37:17172–9. http://dx.doi.org/10.1016/j.ijhydene.2012.08.023.
[28] Santamaria AD, Bachman J, Park JW. Design strategy for a polymer electrolyte membrane fuel cell flow-field capable of switching between parallel and interdigitated configurations. Int J Hydrogen Energy 2013.
[29] Santamaria AD, Cooper NJ, Becton MK, Park JW. Effect of channel length on interdigitated flow-field PEMFC performance: a computational and experimental study. Int J Hydrogen Energy 2013;38:16253–63.
[30] Berning T, Lu DM, Djilali N. Three-dimensional computational analysis of transport phenomena in a PEM fuel cell. J Power Sources 2002;106:284–94. http://dx.doi.org/10.1016/S0378-7753(01)01057-6.
[31] Gurau V, Barbir F, Liu H. An analytical solution of a half-cell model for PEM fuel cells. J Electrochem Soc 2000;147:2468–77. http://dx.doi.org/10.1149/1.1393555.
[32] Nield DA. The boundary correction for the Rayleigh-Darcy problem: limitations of the Brinkman equation. J Fluid Mech 1983;128:37–46. http://dx.doi.org/10.1017/S0022112083000361.
[33] Gostick JT, Fowler MW, Pritzker MD, Ioannidis MA, Behra LM. In-plane and through-plane gas permeability of carbon fiber electrode backing layers. J Power Sources 2006;162:228–38. http://dx.doi.org/10.1016/j.jpowsour.2006.06.096.
[34] Sigracet. GDL 10 Series Gas Diffusion Layer 2007: Material Data Sheet.
[35] Patterson TF, Rudman IK. Water and air permeability of wet sheets. Project F002, report 6: a progress report to member companies of the Institute of Paper Science and Technology; 1998.
[36] Jiao K, Li X. Water transport in polymer electrolyte membrane fuel cells. Prog Energy Combust Sci 2011;37:221–91. http://dx.doi.org/10.1016/j.pecs.2010.06.002.
[37] Baghalha M, Eikerling M, Stumper J. The effect of MPL permeability on water fluxes in PEM fuel cells: a lumped approach. ECS Trans 2010;33:1529–44. http://dx.doi.org/10.1149/1.3484645.
[38] Cooper K. Characterizing through-plane and in-plane ionic conductivity of polymer electrolyte membranes. ECS Trans 2011;41:1371–80. http://dx.doi.org/10.1149/1.3635668.
[39] Danilov VA, Tade MO. An alternative way of estimating anodic and cathodic transfer coefficients from PEMFC polarization curves. Chem Eng J 2010;156:496–9. http://dx.doi.org/10.1016/j.cej.2009.09.022.
[40] Wang JX, Uribe FA, Springer TE, Zhang J, Adzic RR. Intrinsic kinetic equation for oxygen reduction reaction in acidic media: the double Tafel slope and fuel cell applications. Faraday Discuss 2009;140:347–62. http://dx.doi.org/10.1039/B802218F.
[41] Al-Hussainy R, Ramey Jr HJ, Crawford PB. The flow of real gases through porous media n.d. http://dx.doi.org/10.2118/1243-A-PA.